

## Probability-Based Diagnostic Imaging Technique Using Error Functions for Active Structural Health Monitoring

Rahim Gorgin, Zhanjun Wu, Yuebin Zheng

State Key Laboratory of Structural Analysis for Industry Equipments, School of Aeronautics and Astronautics, Dalian University of Technology, Dalian 116024, Liaoning, China

### ABSTRACT

This study presents a novel probability-based diagnostic imaging (PDI) technique using error functions for active structural health monitoring (SHM). To achieve this, first the changes between baseline and current signals of each sensing path are measured, and by taking the root mean square of such changes, the energy of the scattered signal at different times can be calculated. Then, for different pairs of signal acquisition paths, an error function based on the energy of the scattered signals is introduced. Finally, the resultant error function is fused to the final estimation of the probability of damage presence in the monitoring area. As for applications, developed methods were employed to various damage identification cases, including cracks located in regions among an active sensor network with different configurations (pulse-echo and pitch-catch), and holes located in regions outside active network sensors with pitch-catch configuration. The results identified using experimental Lamb wave signals at different central frequencies corroborated that the developed PDI technique using error functions is capable of monitoring structural damage, regardless of its shape, size and location. The developed method doesn't need direct interpretation of overlaid and dispersed lamb wave components for damage identification and can monitor damage located anywhere in the structure. These bright advantages, qualify the above presented PDI method for online structural health monitoring.

**Keywords** - Probability-based diagnostic imaging, Structural health monitoring, Lamb waves, Piezoelectric transducers, Scattered signal energy, Error function

### I. INTRODUCTION

To ensure structural integrity and hence maintain safety during service, active SHM techniques have found important roles throughout the aerospace, mechanical, and civil engineering communities. Traditional non-destructive evaluation (NDE) techniques (e.g. X-ray imaging, ultrasonic scans, infrared thermography, acoustic wave propagation, and eddy current) are somehow difficult to implement, and some of them are impractical in many cases such as in-service aircraft testing and in situ space structures. In contrast, SHM is an emerging technology with intelligent algorithms to interrogate the 'health' condition of structures in real time or whenever necessary [1]. Lamb waves (ultrasonic guided waves that propagate inside thin-wall plates and shallow shells) have been increasingly employed to develop various SHM techniques [1-10]. As Lamb waves travel long distances in structure and can be applied with conformable piezoelectric (PZT) actuators/sensors that require little power, they are suitable for structural health monitoring [11].

Recently, there has been increasing interest in introducing probability-based diagnostic imaging (PDI) techniques to lamb wave based SHM. A PDI method attempts to describe a damage event using an image. The field value at each image pixel shows the

probability of damage presence at that point [12]. PDI techniques present damage in terms of its presence probability. Temporal-information-based PDI techniques use the time-of-flight (TOF) of damage-scattered wave packets to spatial loci reflecting the possibility of damage presence in each point of the structure, and then applies geometric triangulation to locate the damage [13-17]. Such techniques are able to identify the location of damages anywhere in the structure. However it is quite difficult to extract this kind of damage-sensitive feature due to the complex mechanisms of lamb wave propagation in structures, even with a large number of sophisticated signal processing techniques.

Signal-correlation-based PDI presumes that a low correlation between baseline and current signal indicates a high probability of damage presence along the sensing path, and that the damage can be monitored by seeking intersections of several paths along which the collected signals show low correlation [18-20]. These methods do not need complicated signal interpretation nevertheless they are able to highlight damage located in the region among the transducers.

This study developed an appropriate probability-based diagnostic imaging algorithm for active SHM. To this end, changes in Lamb wave signals between the current and baseline signal were measured.

Subsequently, the energy of the scattered signals at different times was calculated by taking the root mean square of such signals. For different pairs of signal acquisition paths an error function based on the energy of their scattered signals is introduced. The resultant error function then is used to construct the probability image in the monitoring area. To validate the presented algorithm, experimental evaluations are conducted at different central frequencies, including monitoring cracks located in regions among an active sensor network with different configurations (pulse-echo and pitch-catch) and a hole located in a region outside an active network sensor with pitch-catch configuration, demonstrating the potential of such a PDI algorithm for identifying damage in structures. A good advantage of this developed technique is its capability of highlighting damage anywhere in the plate (not necessarily located in the region between transducers) without any need for interpretation of collected signals.

## II. METHODOLOGY

In this paper, a new PDI method for active SHM is developed by analyzing the scattered waves induced at structural flaws. If lamb wave incident with a damage, scattering will occur in all directions. Therefore, damage can be considered as a wave scattering source. Fig. 1 illustrates this approach. For a given network of  $N$  sensors and  $N$  actuators, the baseline and current line are collected for all sensing paths. The Short time Fourier transform (STFT) which are sufficient for analysis and visualization of lamb wave signals, is used to extract beneficial diagnostic information. The Short time Fourier transform of a raw signal  $f(t)$  is defined as:

$$f(\omega, t) = \frac{1}{2\pi} \int_{-\infty}^{\infty} e^{-i\omega\tau} f(\tau)h(\tau-t)d\tau \quad (1)$$

Where,  $h(t)$ , is the window function.

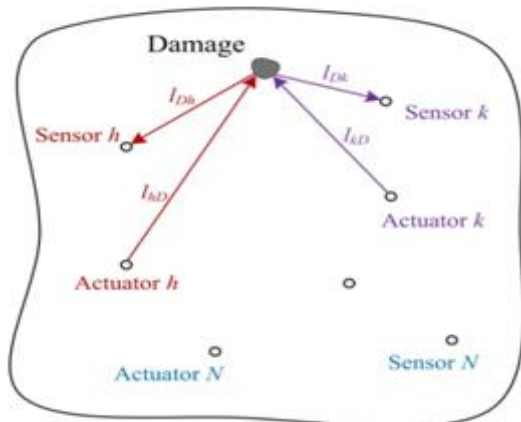


Fig. 1: Diagnostic approach

According to baseline and current signals, the scattered response of each path is determined at driving frequency ( $\omega = \omega_0$ ). As illustrated in Fig. 1, the time of flights  $TOF_h$ , of the path  $h$  should correspond to the wave travel time from Actuator  $h$  to the damage and then from the damage to Sensor  $h$  and  $TOF_k$ , is the wave travel time from Actuator  $k$  to the damage and then from the damage to Sensor  $k$  such that:

$$l_{hD} + l_{Dh} = c(TOF_h) \quad (2)$$

$$l_{kD} + l_{Dk} = c(TOF_k) \quad (3)$$

Where,  $l_{hD}$ ,  $l_{kD}$ ,  $l_{Dh}$  and  $l_{Dk}$  are the linear distance between damage and Actuator  $h, k$ , Sensor  $h$  and  $k$  respectively.  $c$ , is the wave velocity. Assuming the wave velocity before and after incident is constant and the same for all paths, then based on equation (2) and equation (3) it can be written:

$$\frac{l_{hD} + l_{Dh}}{l_{kD} + l_{Dk}} = \frac{TOF_h}{TOF_k} \quad (4)$$

Since it is quite difficult to extract TOF due to the complex mechanism of lamb wave propagation in engineering structures, an alternative feature is introduced while its extraction does not need any interpretation of the signals. To achieve this, for both paths, the energy of the scattered signal at different times can be computed by taking the root mean square (RMS) of scattered response as follows:

$$RMS(t_i) = \sqrt{\frac{\sum_{e=0}^i s(\omega_0, t_e)^2}{Z}} \quad (5)$$

Here,  $RMS(t_i)$  is the energy of the scatter signal till  $(t = t_0)$ ,  $s(\omega_0, t_e)$  is the amplitude of the scatter signal at  $(t = t_0 \text{ and } \omega = \omega_0)$ , and  $Z$  is the number of data points.

As illustrated in Fig. 2, the energy of the scatter signals of paths  $h$  and  $k$  respectively, at times  $TOF_h$  and  $TOF_k$  starts to increase. Based on the distance of each path to the damage and also to the structure boundaries, normalized scatter signal energy at different times reach a definite value. Although the times at which both paths reach a definite value of the scatter signal energy are different from their time of flights, still their ratio is close to the ratio of their time of flights (especially when sensing paths are far from structure boundaries) such that:

$$\frac{TOF_h}{TOF_k} \cong \frac{t_h(RMS_i)}{t_k(RMS_i)} \quad 0 < RMS_i < \beta_{hk} \quad (6)$$

Where,  $t_h(RMS_i)$  and  $t_k(RMS_i)$  are the times when the normalized scatter signal energy of paths  $h$  and  $k$  reach to the value,  $RMS_i$ , respectively. As shown in Fig. 2,  $\beta_{hk}$ , denotes a threshold level for the scatter signal energy to be used in equation (6) because, for the scatter signal energy values more than  $\beta_{hk}$ ,  $t_h(RMS_i)$  cannot be defined. Substituting equation (6) into equation (4) leads to:

$$\frac{l_{hD} + l_{Dh}}{l_{kD} + l_{Dk}} \cong \frac{t_h(RMS_i)}{t_k(RMS_i)} \quad 0 < RMS_i < \beta_{hk} \quad (7)$$

According to the differences between the ratio of time of flights and the ratio of times which paths reach to definite scatter signal energy, an error function is introduced with respect to equation (7) as follow:

$$\varepsilon_{hk} = \frac{\sum_{i=0}^{\beta_{hk}} \left| (l_{hD} + l_{Dh}) - \left[ \frac{t_h(RMS_i)}{t_k(RMS_i)} \times (l_{kD} + l_{Dk}) \right] \right|}{M} \quad (8)$$

Here,  $M = \beta_{hk} / \Delta s$ , is the number of samples according to the sampling period ( $\Delta s$ ) of the scattered signal energy. The monitoring area is meshed into uniformly distributed grids and the error function is determined for each grid. Grids with the minimum values of the error function show the most probable location of damage. In order to find the exact location of damage, other error functions must be defined with respect to different signal acquisition paths. Using more error functions decreases the effects of measurement noise and uncertainties and increases the accuracy of the proposed algorithm.

For a sensor network with  $R$  sensing paths,  $a = \sum_{i=1}^R (P(i) - 1)$  ( $P = [2, 3, \dots, R]$ ) error

functions can be defined. Eventually, the resultant error function is defined by:

$$\varepsilon = \sqrt{\sum_{j=1}^a \varepsilon_j^2} \quad (9)$$

The resultant error function is used to estimate the probability of the presence of damage in the structure. Grids with the minimum value of the resultant error function highlight the most probable location of damage.

### III. APPLICATION TO STRUCTURAL DAMAGE IDENTIFICATION

The presented probability-based diagnostic imaging method was employed to identify two common types of damages in aluminum plates, including through-thickness cracks and holes, by using different active sensor networks.

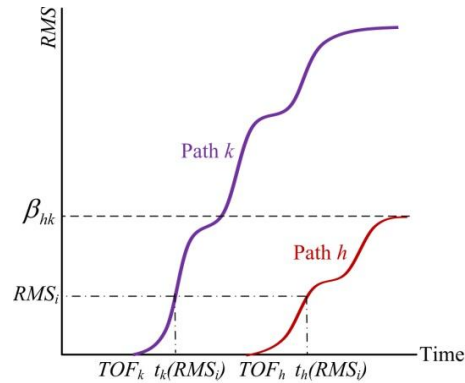


Fig. 2: The growth of scattered signals energy

### 3.1 Crack, using an active sensor network with pulse-echo configuration

An aluminum plate (500 mm × 500 mm × 3 mm) was fixed along its four edges on a testing table, and a through-thickness crack (30 mm long and 1.5 mm wide) was introduced into the plate, as seen in Fig. 3.

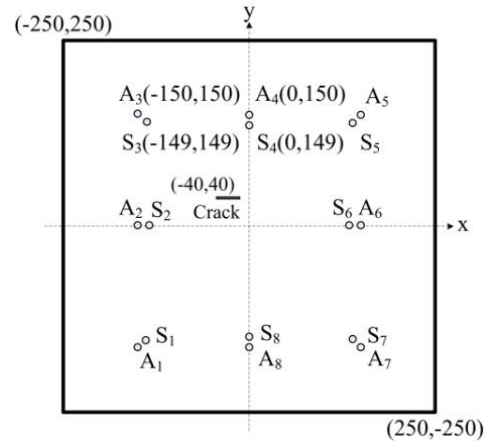


Fig. 3: Schematic diagram of aluminum plate with a crack (dimensions in mm)

Table 1: Material properties of PZT transducer

Product name	APC 851
Geometry (mm)	( $\phi = 6.6$ and $h_{PZT} = 0.24$ )
Density ( $g/cm^3$ )	7.6
Electromechanical coupling factor $k_p$	0.71
Voltage constant $g_{33}$ (Vm / N)	$24.8 \times 10^{-3}$
Charge constant $d_{33}$ (m / V)	$400 \times 10^{-12}$
Relative dielectric constant $k^T$	1950
Frequency constant $N_T$ (Hz . m)	2040
Elastic constant $E$ (GPa)	63

The active sensor network with pulse-echo configuration was set up with sixteen surface-mounted piezoelectric discs (APC 851) of 6.6 mm in diameter and 0.24 mm in thickness. Piezoelectric discs properties are given in Table. 1. The active network sensor provided eight pulse-echo sensing paths,  $A_i - S_i$  ( $i = 1, 2, \dots, 8$ ). Generation and acquisition of lamb waves were fulfilled using a Scan Genie machine. A 5-cycle sinusoidal toneburst enclosed in a Hanning window at a central frequency of 150 kHz was generated and acquired at a sampling rate of 48 MHz. Sampled signals were transmitted into the central processing unit for further analysis. All the diagnosis control and signal analysis was performed using a central processing unit. Different central frequencies (200 kHz and 250 kHz) were also used to validate the robustness of the PDI method. The current and baseline signals are captured and the scattered signal of each sensing path is defined. As an example, the scattered signal of sensing paths  $A_4 - S_4$  and  $A_8 - S_8$  are shown in Fig. 4.

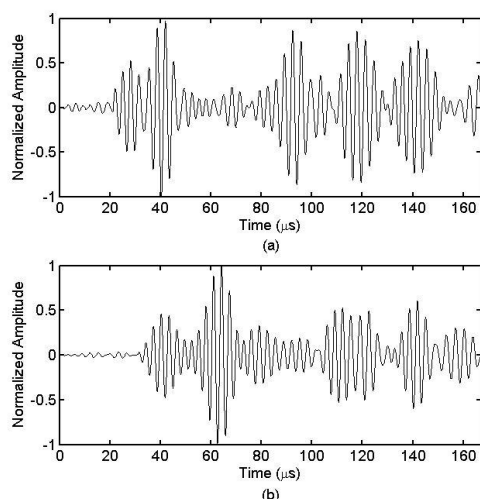


Fig. 4: Scattered signals acquired via pulse-echo sensing paths (Normalized by the maximum magnitude of each scattered signal): (a)  $A_4 - S_4$ ; (b)  $A_8 - S_8$

The RMS values of the scattered signals at different times are determined by equation (5). Fig. 5 exemplarily illustrates the energy of the scattered signals at different times obtained from sensing paths  $A_4 - S_4$  and  $A_8 - S_8$ . The RMS values are normalized. A function is defined for this network. Figure 6 exhibits the error function  $\epsilon_{48}$  defined based on sensing paths  $A_4 - S_4$  and  $A_8 - S_8$ . The probability values were normalized. As can be seen in Fig. 6, grids with the minimum values of error

function  $\epsilon_{48}$ , highlight locations with the most probability of presence damage.

Finally, the resultant error function for each grid is calculated and shown in Fig. 7. The location of the actual crack is shown in the image and the central location of identified crack (the grid with the minimum value of the resultant error function) is marked by 'x'. The probability values were normalized.

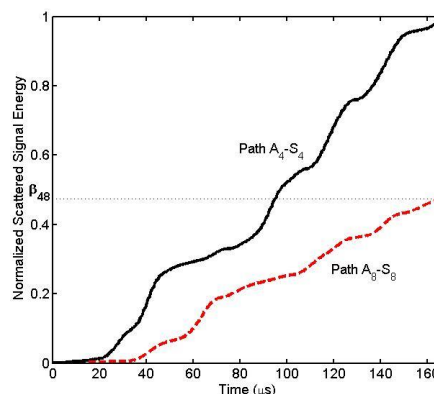


Fig. 5: The energy of scattered signals  $A_4 - S_4$  and  $A_8 - S_8$  till different times (Normalized by the ultimate energy magnitude of sensing path  $A_4 - S_4$ )

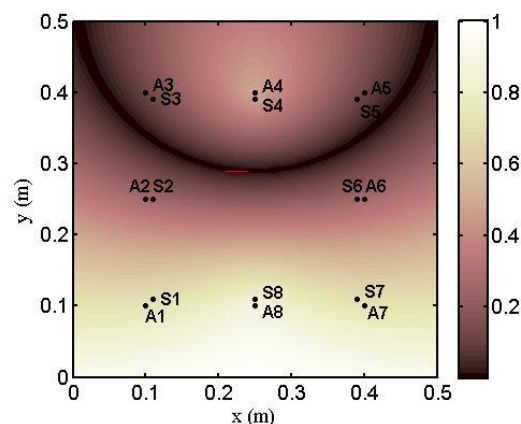


Fig. 6: The values of error function  $\epsilon_{48}$  defined based on pulse-echo sensing paths  $A_4 - S_4$  and  $A_8 - S_8$  (Normalized by the maximum magnitude of error function  $\epsilon_{48}$ )

As shown in Fig. 7, the central location of the identified crack at different central frequencies is close to actual location of the crack which proves the efficiency of the presented method in damage diagnostic.

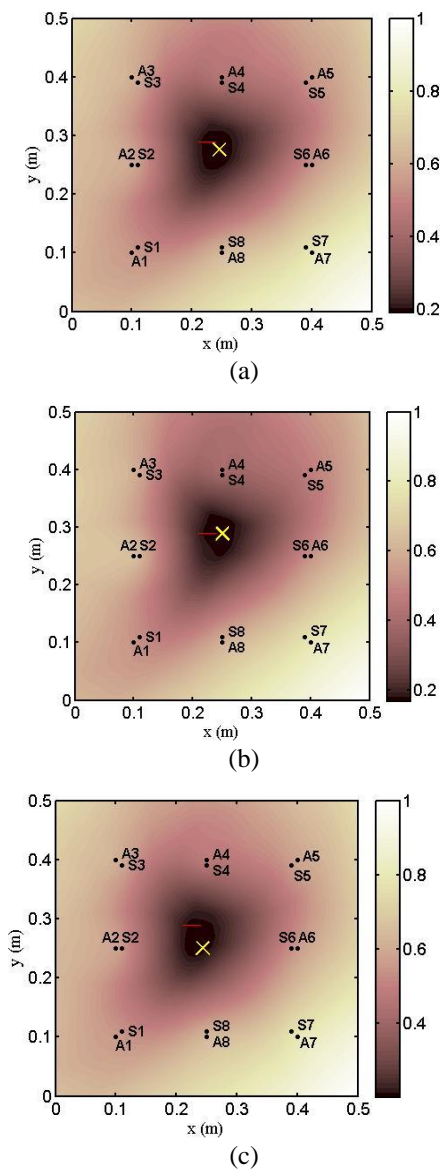


Fig. 7: Ultimate resulting image (the resultant error function values) for crack using a sensor network with pulse-echo configuration in different central frequencies (Normalized by the maximum magnitude of resultant error function): (a) 150 KHz; (b) 200 KHz; (c) 250 KHz

### 3.2 Crack, using an active sensor network with pitch-catch configuration

As an extension of the above application, the approach was used to identify the crack described in previous section, via active sensor network with pitch-catch configuration. The active network sensor provide 56 pulse-echo sensing paths,  $A_i - S_j$  ( $i, j = 1, 2, \dots, 8$  but  $i \neq j$ ).

Therefore, 1540 error functions can be introduced for this network. For different central frequencies, (150, 200 and 250 KHz) all error functions are defined by equation (8) then the resultant error function at each central frequency is calculated for each grid and shown in Fig. 8. As shown in Fig. 8, the more satisfactory identification confidence was achieved for sensor network with pitch-catch configuration. Because sensor network with pitch-catch configuration provides more error functions compared with pulse-echo configuration.

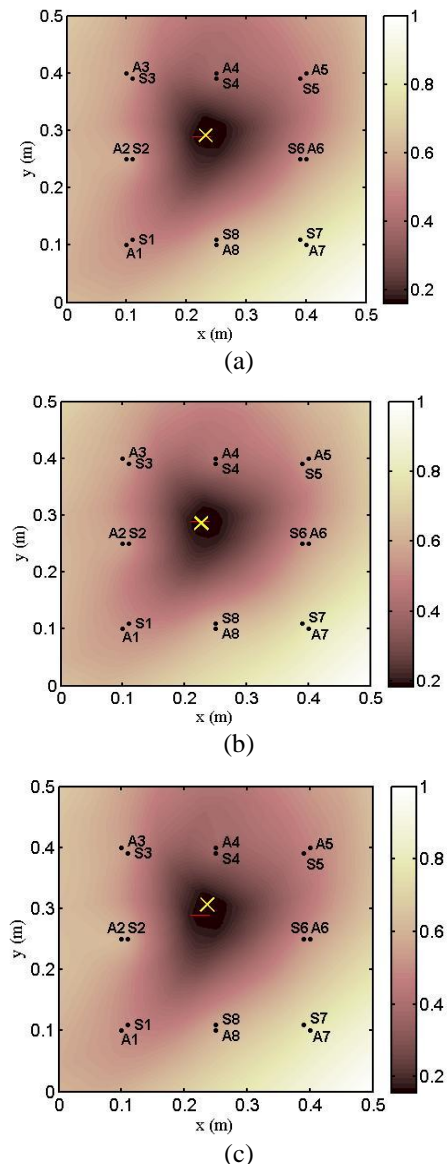


Fig. 8: Ultimate resulting image (the resultant error function values) for crack using a sensor network with pitch-catch configuration in different central frequencies (Normalized by the maximum magnitude of resultant error function): (a) 150 KHz; (b) 200 KHz; (c) 250 KHz

### 3.3 Hole, using an active sensor network with pitch-catch configuration

In order to examine capability of the proposed algorithm in highlighting damage with different shape, size and location, the presented method was used to monitor a hole in aluminum plate. Two sets of sensor network with pitch-catch configuration, each with surface-mounted piezoelectric discs are set up on the aluminum plate to identify a hole which was placed outside the region between transducers, as seen in Fig. 9.

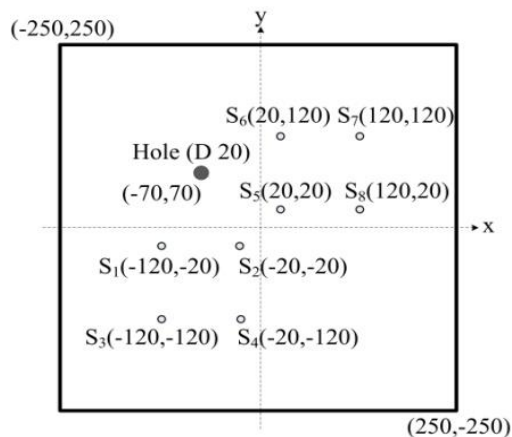


Fig. 9: Schematic diagram of aluminum plate with a hole (dimensions in mm)

Piezoelectric discs acted as both actuators and sensors with the aid of a two-way switch. The active network sensor provided 56 sensing paths accordingly 1540 error functions can be defined for damage identification procedure. For different central frequencies, (150, 200 and 250 KHz) all error functions are obtained by equation (8) and subsequently the resultant error functions are calculated for each grid and shown in Fig. 10.

As shown in Fig. 10, the central location of the identified hole at different central frequencies is close to the location of the actual location of the hole which proves the effectiveness of the developed PDI technique in damage detection regardless the shape, size and location of damage.

### IV. CONCLUSIONS

A probability-based diagnostic imaging technique using error functions for active SHM was evaluated through experimental studies. To this end, error functions are introduced based on the energy of the scattered signals and the resultant error function then is defined to construct the probability image in the monitoring area. Satisfactory results from various damage identification cases, including crack among an active sensor network with different configurations (pulse-echo and pitch-catch) and a hole outside an active network sensor with pitch-catch configuration, at different central frequencies, have demonstrated the effectiveness of the proposed

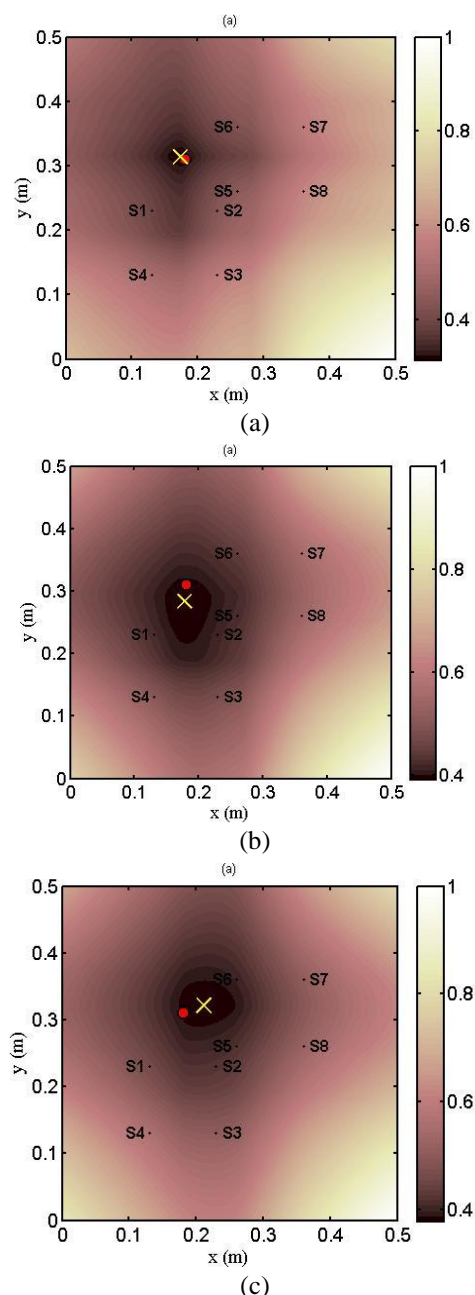


Fig. 10: Ultimate resulting image (the resultant error function values) for hole using a sensor network with pitch-catch configuration in different central frequencies (Normalized by the maximum magnitude of resultant error function): (a) 150 KHz; (b) 200 KHz; (c) 250 KHz

PDI technique in illuminating damage regardless its shape, size and location in the structures. The sensitivity and resolution of this technique depends on the number of error functions which is used to define the resultant error function. Accordingly, since a sensor network with pitch-catch configuration provides more sensing paths and subsequently more error functions, using developed algorithm for a sensor network with pitch-catch configuration gives

more satisfactory results compare with its pulse-echo configuration. Unlike temporal-based-information PDI methods, this developed method doesn't need direct interpretation of overlaid and dispersed lamb wave components for damage identification.

Moreover, unlike signal-correlation-based PDI techniques, via developed algorithm, damage located anywhere in the structure (not necessarily located in region among transducers) can be monitored. These bright advantages, qualify presented PDI method for online structural health monitoring.

## V. ACKNOWLEDGEMENTS

This work was supported by the National Natural Science Foundation of China (11172053 and 91016024) and the New Century Excellent Talents in University (NCET-11-0055) and the Fundamental Research Funds for the Central Universities (DUT12LK33).

## REFERENCES

- [1] J.-B. Ihn and F.-K. Chang, *Pitch-catch active sensing methods in structural health monitoring for aircraft structures*, *Structural Health Monitoring*, 7(1), 2008, 5-19.
- [2] T. Kundu, S. Das and K.V. Jata, *Health monitoring of a thermal protection system using lamb waves*, *Structural Health Monitoring*, 8(1), 2009, 29-45.
- [3] J.-B. Ihn and F.-K. Chang, *Detection and monitoring of hidden fatigue crack growth using a built-in piezoelectric sensor/actuator network: I. Diagnostics*, *Smart Materials and Structures*, 13(3), 2004, 609-620.
- [4] L. Wang and F.G. Yuan, *Damage identification in a composite plate using prestack reverse-time migration technique*, *Structural Health Monitoring*, 4(3), 2005, 195-211.
- [5] Z. Wu and F.-K. Chang, *Damage detection for composite laminate plates with a distributed hybrid PZT/FBG sensor network*, *Intelligent Material Systems and Structures*, 20(9), 2009, 1069-1077.
- [6] H. Sohn and S. J. Lee, *Lamb wave tuning curve calibration for surface-bonded piezoelectric transducers*, *Smart Materials and structures*, 19(1), 2010, 015007.
- [7] C.H. Wang, J.T. Rose and F.-K. Chang, *A synthetic time-reversal imaging method for structural health monitoring*, *Smart Materials and Structures*, 13(2), 2004, 413-423.
- [8] C.H. Wang, J.T. Rose and F.-K. Chang, *A computerized time-reversal method for structural health monitoring*, *Proc. of SPIE Conference on Smart Structures/NDE, San Diego*, 2003, 48-58.
- [9] B. Lin and V. Giurgiutiu, *Modeling and testing of PZT and PVDF piezoelectric wafer active sensors*, *Smart Materials and Structures*, 15(4), 2006, 1085-1093.
- [10] N. Hu, T. Shimomukai, H. Fukunaga and Z. Su, *Damage identification of metallic structures using A0 mode of lamb waves*, *Structural Health Monitoring*, 7(3), 2008, 271-285.
- [11] H. Sohn, G. Park, J. R. Wait, N. P. Limback and C.R. Farrar, *Wavelet-based active sensing for delamination detection in composite structures*, *Smart Materials and structures*, 13(1), 2004, 153-160.
- [12] Z. Su, X. Wang, L. Cheng, L. Yu and Z. Chen, *On selection of data fusion schemes for structural damage evaluation*, *Structural Health Monitoring*, 8(3), 2009, 223-241.
- [13] Z. Su, L. Cheng, X. Wang, L. Yu and C. Zhou, *Predicting delamination of composite laminates using an imaging approach*, *Smart Materials and Structures*, 18, 2009, 074002.
- [14] J. E. Michaels, *Detection, localization and characterization of damage in plates with an in situ array of spatially distributed ultrasonic sensors*, *Smart Materials and Structures*, 17, 2008, 035035.
- [15] G. Konstantinidis, B. W. Drinkwater and P.D. Wilcox, *The temperature stability of guided wave structural health monitoring systems*, *Smart Materials and Structures*, 15, 2006, 967-976.
- [16] Q. Wang and S. F. Yuan, *Baseline-free imaging method based on new PZT sensor arrangements*, *Intelligent Material Systems and Structures*, 20(14), 2009, 1663-1673.
- [17] J.E. Michaels and T.E. Michaels, *Guided wave signal processing and image fusion for in situ damage localization in plates*, *Wave Motion*, 44(6), 2007, 482-492.
- [18] X. Zhao, H. Gao, G. Zhang, B. Ayhan, F. Yan, C. Kwan and J.L. Rose, *Active health monitoring of an aircraft wing with embedded piezoelectric sensor/actuator network: I. Defect detection, localization and growth monitoring*, *Smart Materials and Structures*, 16(4), 2007, 1208-1217.
- [19] W. Ostachowicz, P. Kudela, P. Malinowski and T. Wandowski, *Damage localization in plate-like structures based on PZT sensors*, *Mechanical Systems and Signal Processing*, 23, 2008, 1805-1829.
- [20] D. Wang, L. Ye, Z. Su, Y. Lu, F. Li and G. Meng, *Probabilistic damage identification based on correlation analysis using guided wave signals in aluminum plates*, *Structural Health Monitoring*, 9(2), 2010, 133-144.